ISSN 0023-1584, Kinetics and Catalysis, 2014, Vol. 55, No. 6, pp. 748–762. © Pleiades Publishing, Ltd., 2014.
Original Russian Text © A.S. Ivanova, E.V. Korneeva, E.M. Slavinskaya, D.A. Zyuzin, E.M. Moroz, I.G. Danilova, R.V. Gulyaev, A.I. Boronin, O.A. Stonkus, V.I. Zaikovskii, 2014, published in Kinetika i Kataliz, 2014, Vol. 55, No. 6, pp. 467–482.

Role of the Support in the Formation of the Properties of a Pd/Al_2O_3 Catalyst for the Low-Temperature Oxidation of Carbon Monoxide

A. S. Ivanova[a, *], E. V. Korneeva[a], E. M. Slavinskaya[a], D. A. Zyuzin[a], E. M. Moroz[a], I. G. Danilova[a], R. V. Gulyaev[a], A. I. Boronin[a, b], O. A. Stonkus[a, b], and V. I. Zaikovskii[a, b]

[a] *Boreskov Institute of Catalysis, Siberian Branch, Russian Academy of Sciences, Novosibirsk, 630090 Russia*

[b] *Novosibirsk State University, Novosibirsk, 630090 Russia*

* *e-mail: iva@catalysis.ru*

Received January 30, 2014

Abstract—The Pd/Al_2O_3 catalysts were prepared by the impregnation of aluminum hydroxide, which was synthesized by precipitation in the presence of polyvinyl alcohol, with a solution of palladium nitrate and were heat-treated at different temperatures. The resulting samples were characterized by X-ray diffraction, electron microscopy, diffuse reflectance spectroscopy, and X-ray photoelectron spectroscopy and were tested in CO oxidation in two modes: in a temperature-programmed reaction and under isothermal conditions at 20°C in the absence and in the presence of water vapor. The activity of the catalysts in the former mode was almost independent of support preparation conditions, but it was different in the latter mode. The catalyst whose support was obtained in the presence of polyvinyl alcohol and treated at 300°C in an atmosphere of nitrogen exhibited the highest activity in CO oxidation at 20°C. In the absence of water vapor from the reaction mixture, the initial conversion of CO reached 40% and then decreased. In the presence of water vapor, a continuous increase in the conversion of CO to 88% was observed, and the activity was stabilized at this level. The smallest size of palladium metal nanoparticles, the nearly monolayer carbon surface coverage, and the presence of OH groups, which are formed upon the dissociation of water present in the reaction mixture, facilitate an increase in activity.

DOI: 10.1134/S002315841406007X

INTRODUCTION

Carbon monoxide is an extremely toxic gas because of its ability to be strongly bound to blood hemoglobin more rapidly than oxygen by a factor of 200–300 [1]. The resulting carboxyhemoglobin blocks oxygen transfer and cellular respiration processes. Because the threshold limit value of CO in workplace air is as low as 20 mg/m^3, the removal of CO from waste gases and the atmosphere is a problem of considerable current interest. The low-temperature oxidation of CO at a high humidity of ambient air is of prime importance.

It is well known [2, 3] that supported palladium-containing catalysts, in particular Pd/Al_2O_3, are active in CO oxidation; however, the activity depends on catalyst preparation method and reaction conditions. Ivanova et al. [3] found that the temperature at with a 50% conversion of CO (T_{50}) was reached on the Pd/Al_2O_3 catalysts prepared by the impregnation of a support with a solution of palladium nitrate followed by drying and calcination varied from 135 to 182°C depending on catalyst treatment temperature; that is, these catalysts do not possess low-temperature activity. At the same time, according to Shen et al. [4], the (1.7 wt % Pd + 3.3 wt % $CuCl_2$)/Al_2O_3 catalysts (*CI*), which were prepared with the use of ammonium complexes of palladium and copper, are more active in low-temperature CO oxidation than catalysts prepared by traditional incipient wetness impregnation (*WI*). Thus, 100% CO conversion in a reaction mixture containing 400 ppm of CO and 1000 ppm of H_2O (and the balance air) in the presence of catalyst *CI* was reached even at 0°C. An increase in the water content of the reaction mixture to 6000 ppm led to a decrease in the activity and stability of the catalyst; according to Shen et al. [4], this was due to the condensation of water in the pores of the hydrophilic support.

Use of a hydrophobic support prepared by the formation of a carbon-containing component on its surface under certain synthesis conditions is a method of increasing the resistance of a catalyst to water vapor. For example, magnesium oxide prepared by a sol–gel method [5, 6] contained carbon as a component of $MgO_{2.15–2.64}C_{0.41–0.54}H_{2.80–2.95}$; in this case, the amount of carbon and the temperature of its removal depend on the carbon chain length (methyl, ethyl, propyl, etc.) and the nature of the carbon component (propyl, isopropyl, neopentyl, etc.) [7]. Furthermore, it was found [8] that use of a support precipitated in the presence of the complexing component Pluronic P123

$[HO(CH_2CH_2O)_{20}(CH_2CH(CH_3)O)_{70}(CH_2CH_2O)_{20}H]$ resulted in the formation of more active catalysts for CO oxidation: on the samples of 6 wt % CuO)/$Ce_{1-x}Ti_xO_2$ (x from 0.1 to 0.5), the temperature T_{50} was 60–73°C depending on x. Therefore, it is of special interest to study the effect of surfactants, in particular, polyvinyl alcohol $[-CH_2CH(OH)CH_2CH(OH)-]_n$, introduced at the alumina support synthesis stage, on the properties of the Pd/Al_2O_3 catalyst.

The aim of this work was to study the effects of the preparation conditions and the treatment temperature of an Al_2O_3 support on the physicochemical and catalytic properties of the Pd/Al_2O_3 catalyst in low-temperature CO oxidation.

EXPERIMENTAL

Sample Preparation

The synthesis of catalysts for the low-temperature oxidation of CO included the following operations:

(1) Preparation of the support.

Aluminum oxide was synthesized by the following two methods:

(a) Precipitation from a solution of aluminum nitrate with an aqueous solution of ammonium bicarbonate NH_4HCO_3 (ρ = 1.055–1.064 g/cm^3) in the presence of 40 wt % polyvinyl alcohol (PVA) at constant pH 7.0–7.2 and a temperature of 30°C with the subsequent thermostating at 90°C for 3 h. The resulting suspension was filtered, and the precipitate was washed with distilled water and dried initially in air at room temperature and then at 110°C for 16–18 h; thereafter, it was additionally heat-treated at 300 and 550°C in a flow of nitrogen for 4 h. Henceforth, the resulting samples are designated Al_2O_3(PVA-T-N), where T refers to a temperature of 110, 300, or 550°C, and N refers to nitrogen;

(b) Precipitation from a solution of aluminum nitrate with an aqueous solution of ammonia at constant pH 7.0–7.2 and a temperature of 70°C with the subsequent thermostating for 3 h. The precipitate was filtered off, washed with distilled water until the absence of nitrates, dried at 110°C for 12–14 h and thermally treated in a flow of dried air at 300°C for 4 h. The reference sample is designated Al_2O_3(300-A), where A refers to air.

(2) Supporting of palladium.

The synthesized supports were impregnated with a solution of palladium nitrate. In order to introduce an additional carbon-containing component with two hydrophobic groups, they were pretreated with a solution of dimethylformamide (DMF) $[HCON(CH_3)_2]$. After the impregnation, the samples were treated with a solution of sodium formate $NaHCO_2$ at 80°C, filtered off, washed to remove sodium, and dried at room temperature.

Characterization Methods

The support and catalyst samples were studied by a set of physical methods.

Atomic absorption spectrometry was used for determining the concentrations of main components; the determination error was 0.01–0.03% [9].

X-ray diffraction (XRD) patterns were obtained on a D-500 diffractometer (Siemens, Germany) using monochromatic CuK_α radiation (λ = 1.5418 Å, point-by-point scanning, 2θ = 10° to 75°, 0.05° increments, counting time of 3–5 s per data point). The calculated interplanar spacing d and diffraction peak intensities I_i were compared with the corresponding values from the JCPDS database [10].

The radial electron density distribution (REDD) or radial atomic distribution (RAD) method was used for evaluating the phase compositions of the highly dispersed support and a catalyst on its basis [11]. The intensity of scattered X-radiation over the wide 2θ range from 2° to 155° was measured with a high accuracy by the RAD method using a short wavelength. The application of a powerful synchrotron source of X-radiation—synchrotron radiation—made it possible not only to shorten the exposure time but also to enhance the experimental accuracy. The diffraction patterns were recorded at the High-Resolution Diffractometry and Anomalous Scattering of Synchrotron and Terahertz Radiation Station of the Siberian Center for Synchrotron Radiation (Budker Institute of Nuclear Physics, Siberian Branch, Russian Academy of Sciences) with the use of a Si (1.1.1) crystal monochromator on the diffraction beam with the degree of monochromatization $\Delta\lambda/\lambda \approx 10^{-4}$ (λ = 0/0699 nm). The REDD curves calculated based on experimental data on the scattering of X-rays were compared with the model curves for phases with known structures, which were hypothetical sample constituents. The principle of the construction of model curves made it possible not only to refine the phase composition of the samples but also to reveal the structure peculiarities of their component phases [12]. Furthermore, partial curves, which gave information on the active constituent, were used for analysis.

The electron microscopic studies of the samples were conducted on a JEM-2010 high-resolution transmission electron microscope (HRTEM) (JEOL, Japan) (resolution, 0.14 nm; accelerating voltage, 200 kV). The concentrations of elements and ratios between them were determined by energy-dispersive X-ray microanalysis (EDX) on an EDAX spectrometer (JEOL, Japan) with a resolution of 140 eV and a probe diameter of 10 nm. The samples were applied to a carbon film supported on copper grid.

The specific surface areas of the samples were measured using the thermal desorption of argon [13]; the error was ±10%.

The diffuse reflectance spectra (DRSs) of the samples in the ultraviolet and visible ranges were measured

Table 1. Properties of the supported Pd-containing catalysts differing in preparation methods and support treatment temperatures

Sample	Concentration of Pd, wt %	S_{BET}, m^2/g
Pd/Al_2O_3(PVA-110-N)	1.00	125
Pd/Al_2O_3(PVA-300-N)	1.00	545
Pd/Al_2O_3(PVA-550-N)	1.00	495
Pd/Al_2O_3(300-A)	1.02	307

Table 2. Catalytic activity of the samples in CO oxidation

Catalyst	T_{10}, °C	T_{50}, °C	T_{90}, °C
Pd/Al_2O_3(PVA-110-N)	133	145	163
Pd/Al_2O_3(PVA-300-N)	124	142	150
Pd/Al_2O_3(300-A)	157	165	172

in air without preliminary sample preparation with the aid of a UV-2501 PC spectrometer (Shimadzu, Japan) in the spectral range 11000–54000 cm^{-1} using an IRS-250A diffuse reflectance attachment. Before the measurement of the spectra, powdered catalysts were placed in a quartz cell with an optical path length of 2 mm. The experimentally found reflectances (R) were converted into Kubelka–Munk units $F(R)$ using the equation $F(R) = (1 - R)^2/2R$ [14]. The radiation wavelength used (190–900 nm) was much greater than the particle size of the samples; thus, the electronic properties were averaged over the entire volume of a catalyst particle.

The X-ray photoelectron spectra (XPSs) were measured on an ES 300 spectrometer (Kratos Analytical, Japan) with the use of MgK_α radiation ($h\nu$ = 1253.6 eV) [15–17]. The samples were preliminarily ground in an agate mortar and applied to an indium support. For evaluating the qualitative composition of the surface and detecting the presence of impurities, survey spectra were obtained in a range from 0 to 1100 eV with a step of 1 eV at an analyzer transmission energy of 50 eV. The quantitative composition of the surface and the charge states of the elements were determined by obtaining the precision spectra of individual photoelectron lines with a step of 0.1 eV at an analyzer transmission energy of 25 eV. The experimental spectra were calibrated using the C1s line, whose binding energy was taken to be 285.1 eV. The chemical composition of the samples was calculated from the integrated intensity of lines or their components taking into account atomic sensitivity factors [18].

The catalytic properties of the samples were studied in an automated system with a flow reactor using mass spectrometry for the analysis of the gas mixture. A catalyst sample with a particle size of 0.25–0.5 mm was placed in a stainless steel reactor and tested in CO oxidation in the following two modes: under conditions of a temperature-programmed reaction (TPR) and under isothermal conditions.

In the TPR mode, the reaction was carried out in a temperature range from –15 to 450°C at a heating rate of 10 K/min with the subsequent cooling in a flow of helium. The reaction mixture containing 0.2 vol % CO, 1.0 vol % O_2, and 0.5 vol % Ne (the balance helium) was supplied a rate of 1000 cm^3/min; the catalyst volume was 0.25 cm^3.

In the isothermal mode at a temperature of 20°C, the reaction mixture containing either 100 ppm of CO, 1.0 vol % O_2, and 0.5 vol % Ne (balance helium) or 100 ppm of CO, 1.0 vol % O_2, 0.5 vol % Ne, and 2.3 vol % H_2O, which corresponds to the pressure of water vapor at 20°C (balance helium) was supplied to the initial catalyst with a volume of 0.6 cm^3 cooled to 20°C at a rate of 200 cm^3/min.

Changes in the composition of the reaction mixture in the course of reaction were monitored by mass spectrometry using neon as the reference permanent gas. The concentrations of CO, O_2, CO_2, and H_2O at each point were measured with a frequency of 0.34 Hz (at regular intervals of 2.94 s). The conversion of CO was calculated from the formula $x = (C^0_{CO} - C^к_{CO})/C^0_{CO}$, where x is the CO conversion, and C^0_{CO} and $C^к_{CO}$ are the initial and final concentrations of CO, respectively.

RESULTS AND DISCUSSION

Chemical Composition of the Samples

According to the results of chemical analysis (Table 1), the palladium content of all of the test samples was ~1.0 wt %. The specific surface area (S_{BET}) of the Pd/Al_2O_3(PVA) catalysts depended on the support treatment temperature (110, 300, or 550°C). Pd/Al_2O_3(PVA-300-N) exhibited a maximum specific surface area of 545 m^2/g, which is larger than the S_{BET} of the Pd/Al_2O_3(300-A) sample by a factor of about 1.7.

Catalytic Properties of the Samples

Table 2 summarizes the results of studying the activity of the supported Pd-containing catalysts, which differed in preparation methods and support treatment temperatures, in CO oxidation under TPR conditions. The temperatures T_{10}, T_{50}, and T_{90} increased both with decreasing the treatment temperature of the Al_2O_3(PVA-N) support from 300 to 100°C and upon the replacement of Al_2O_3(PVA-300-N) by Al_2O_3(300-A); however, differences in the activity of the samples were small. The temperatures at which the CO conversion reached 10 and 50% were 124 and 142 or 157 and 165°C on the Pd/Al_2O_3(PVA-300-N) or Pd/Al_2O_3(300-A) sample, respectively. Thus, the catalysts on the support prepared in the presence of PVA

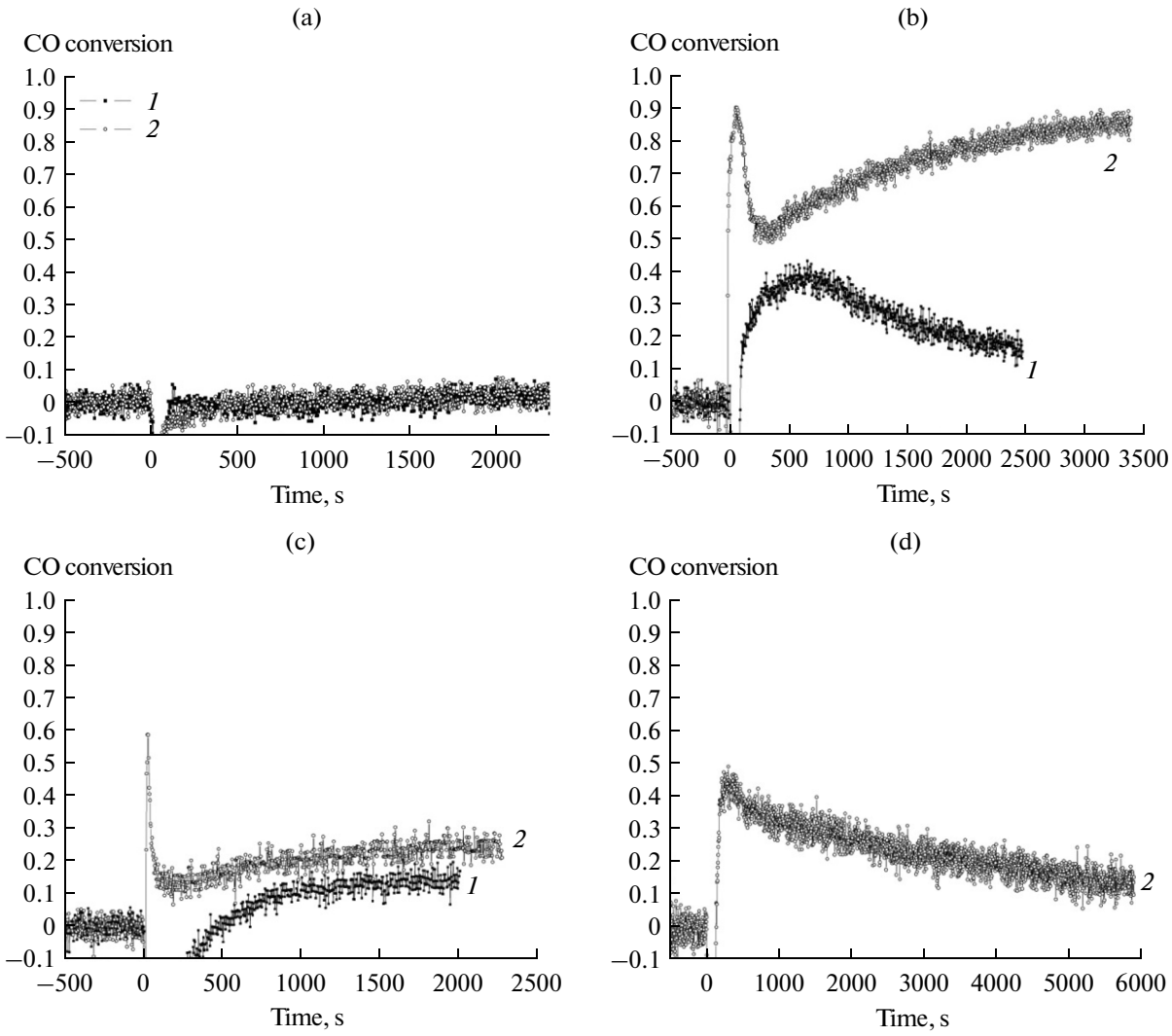

Fig. 1. The time dependence of CO conversion (*1*) in the absence and (*2*) in the presence of water vapor on the (a) Pd/Al_2O_3(PVA-110-N), (b) Pd/Al_2O_3(PVA-300-N), (c) Pd/Al_2O_3(PVA-550-N), and (d) Pd/Al_2O_3(300-A) catalysts.

were more active in CO oxidation performed at a high space velocity of 240 000 h^{-1} and a high CO concentration of 0.2 vol %, but only at temperatures higher than 100°C.

The same catalysts were tested under isothermal conditions in the absence and in the presence of water vapor at a reaction temperature of 20°C and lower space velocity (20 000 h^{-1}) and CO concentration (100 ppm). They were different in activity according to the experimental results (Fig. 1).

The Pd/Al_2O_3(PVA-110-N) catalyst was almost inactive both in the absence and in the presence of water in the reaction mixture (Fig. 1a). An increase in the support treatment temperature to 300°C led to an increase in the activity of Pd/Al_2O_3(PVA-300-N) (Fig. 1b): in the absence of water, the initial CO conversion was ~40%; thereafter, it began to decrease; however, in the presence of water, the conversion of CO increased for 45 min and stabilized at a level of 88%. The calcination of the support at a higher temperature caused a decrease in the activity of Pd/Al_2O_3(PVA-550-N): the conversion of CO was ~15 or about 25% in the absence or in the presence of water, respectively (Fig. 1c). A similar change in the CO conversion was also observed on the Pd/Al_2O_3(300-A) reference catalyst (Fig. 1d): in the presence of water, the conversion of CO at the initial point in time was ~50% and then rapidly decreased. Thus, Pd/Al_2O_3(PVA-300-N), whose support was obtained in the presence of PVA with the subsequent calcination in a flow of N_2 at 300°C, was the most active catalyst capable of oxidizing CO at room temperature.

To reveal the reasons for different activity of the catalysts in the absence and in the presence of water vapor in the reaction mixture, it is necessary to compare their properties before and after performing CO oxidation on them. For this purpose, the initial sam-

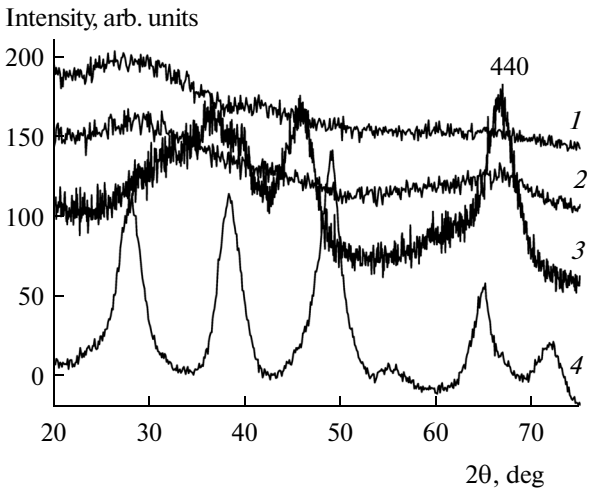

Fig. 2. Diffraction patterns of the (*1*) Al_2O_3(PVA-110-N), (*2*) Al_2O_3(PVA-300-N), (*3*) Al_2O_3(PVA-550-N), and (*4*) Al_2O_3(300-A) supports.

ples and the catalysts subjected to the action of a reaction atmosphere were studied using a set of physical methods. Because the Pd content and the method of supporting palladium were the same in all cases, this allowed us to evaluate the effect of support preparation conditions on the properties of catalysts.

Phase Composition of the Samples

Figure 2 shows the X-ray diffraction patterns of the prepared supports. Aluminum oxide obtained in the presence of PVA after treatment at 110 and 300°C was X-ray amorphous (Fig. 2, curves *1*, *2*). After treatment at 550°C, this was γ-Al_2O_3 (Fig. 2, curve *3*) with a unit cell parameter of 0.7933 nm, which is much greater than the tabulated value of 0.7911 nm; in this case, its particle size determined by XRD analysis did not exceed 3 nm. Consequently, the introduction of PVA at the stage of aluminum hydroxide precipitation followed by treatment at 110 and 300°C facilitated its amorphization. Only after calcination at 550°C, highly dispersed γ-Al_2O_3 with a specific surface area of 495 m^2/g was formed (Table 1). Unlike the above supports, the Al_2O_3(300-A) sample, which was prepared by a traditional method, contained a pseudoboehmite phase (Fig. 2, curve *4*); this is not surprising because pseudoboehmite dehydration with the formation of γ-Al_2O_3 occurs at temperatures of 440–450°C [19].

The treatment of the supports with a solution of DMF did not change the phase composition, as confirmed by the XRD analysis data (Fig. 3a). According to previously published data [3], the supporting of 1 wt % Pd onto γ-Al_2O_3 does not change the phase composition of the support in the catalyst. However, we found that, after the supporting of the same amount of Pd onto aluminum hydroxide preliminarily treated with a solution of DMF, palladium metal Pd^0 was present on the support surface (Fig. 3b); according to XRD data, the particle size of this palladium was no greater than 5 nm. Therefore, synchrotron radiation, whose penetration depth is larger, was used for refining the phase composition of the Al_2O_3(PVA-300-N) support and the Pd/Al_2O_3(PVA-300-N) catalyst.

The diffraction pattern of the Al_2O_3(PVA-300-N) support obtained with the use of synchrotron radiation (Fig. 4a, curve *1*) shows that the support contained an amorphous phase and badly crystallized γ-Al_2O_3 with the pseudospinel structure, in which the cations are located in the tetrahedral and octahedral holes of the close packing of oxygen, which is partially replaced by OH^- groups mainly on the surface [20]. For γ-Al_2O_3, the size of the coherent scattering region was smaller than 2 nm, and the unit cell parameter was a = 0.797 nm. The value of a higher than the tabulated value (a = 0.7911 nm) can be due to an insufficient accuracy of its determination in the badly crystallized oxide.

The diffraction pattern of the initial Pd/Al_2O_3(PVA-300-N) catalyst (Fig. 4a, curve *2*) contains sharp peaks at 7.0°, 12°–13°, and 14.4° due to a phase of the sodium aluminum hydroxycarbonate $NaAlCO_3(OH)_2$ (PCDMF no. 45-1359) along with spread-out peaks characteristic of the badly crystallized phase of γ-Al_2O_3. In this case, the individual maximums of the Pd^0 phase are not detected (their positions are marked by vertical lines). The shape of the diffraction pattern of the catalyst after its testing in CO oxidation in the presence of water vapor is different from that before the reaction (Fig. 4a, curves *2* and *3*). The catalyst support contained the badly crystallized phase of γ-Al_2O_3 before the reaction, whereas new peaks at 6.35°, 12.7°, and 17.1° due to aluminum hydroxide (a pseudoboehmite phase) with a crystallite size of ~3 nm and the interplanar spacing d = 0.63 nm appeared in the diffraction pattern measured after the reaction (Fig. 4a, curve *3*). Note that the individual maximums of the Pd^0 phase are also absent from the diffraction pattern of the catalyst after the reaction.

More information on the phase composition and the local structure of the catalyst was obtained by the RAD method (Figs. 4b, 4c). Figure 4b shows the difference REDD curves of the Pd/Al_2O_3(PVA-300-N) catalyst before and after conducting CO oxidation on it in the presence of water vapor. It is evident that the curves almost coincide. The results of a simulation of the phase composition of the active constituent and changes in the support are shown in Fig. 4c, which gives the difference REDD curve of the Pd/Al_2O_3(PVA-300-N) catalyst after the reaction and model curves calculated for the assumed phases. As can be seen, the catalyst contains a phase of palladium metal, as evidenced by the interatomic distances r of 0.275, 0.389, 0.476, 0.550, 0.615, and 0.674 nm. Only the area of the first coordination peak of this phase coincides with the area of the corresponding peak of the model curve, whereas the other peaks are much smaller; this fact is indicative of a small size of Pd^0

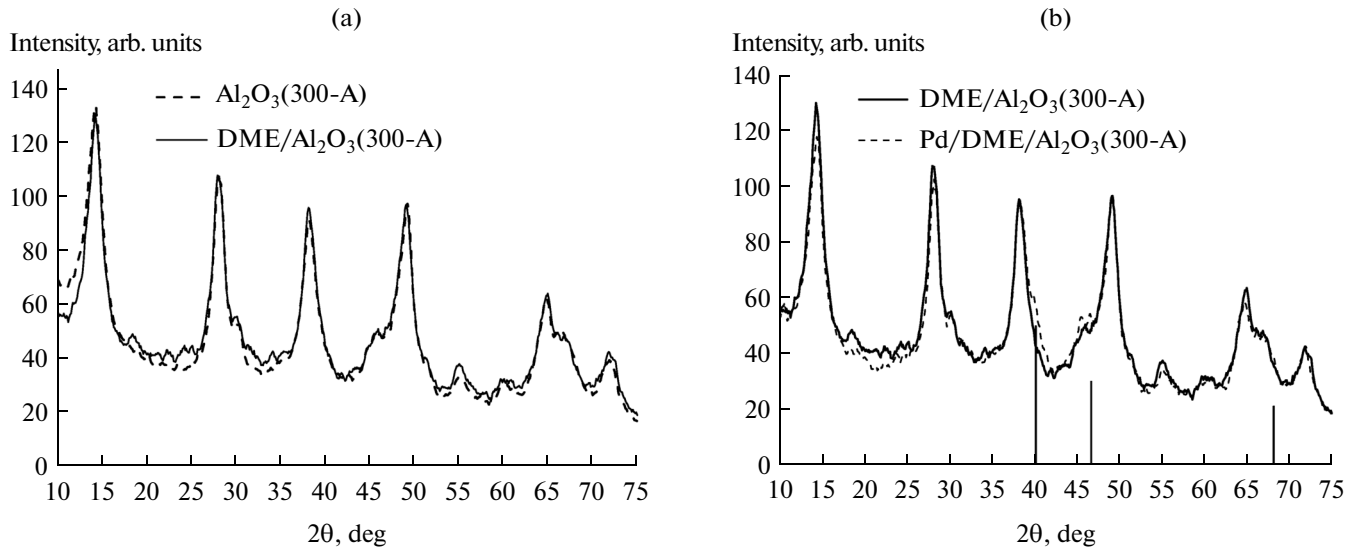

Fig. 3. Diffraction patterns of (a) the Al_2O_3(300-A) support before and after treatment with a solution of DMF and (b) the catalyst based on the treated support. Vertical lines show the positions of the diffraction peaks of Pd^0 (PDMF no. 46-1043).

crystallites, which is no greater than 1 nm according to an estimation.

The difference REDD curve also exhibits minimum r values of 0.18, 0.331, 0.428, and 0.514 nm, whose appearance can be explained by the construction of this curve by subtracting the curve of the initial support, in the structure of which tetrahedral Al–O interatomic distances are present, from the RAD curve of the catalyst, whereas a hydroxide phase free from tetrahedral aluminum appeared in the catalyst after the reaction in addition to the oxide phase. This is confirmed by the agreement of minimum positions in the RAD curve and the partial curve of the oxide, the structure of which contains only tetrahedral interatomic distances (Fig. 4c, curve *4*).

Thus, we used the RAD method to demonstrate that the Pd/Al_2O_3(PVA-300-N) catalyst contained palladium metal both before and after the reaction performed in the presence of water vapor. The crystallite size of palladium metal in this catalyst was no greater than 1 nm, whereas it was ~5 nm in the Pd/Al_2O_3(300-A) catalyst. The support in the Pd/Al_2O_3(PVA-300-N) catalyst was hydrated in the presence of water vapor with the formation of a hydroxide phase of pseudoboehmite. The state of palladium in the test catalysts was also confirmed by the results of electron microscopy.

Electron-Microscopic Analysis of the Samples

According to the electron-microscopic data, the Pd/Al_2O_3(PVA-110-N) sample consists of Pd particles positioned on the support (Fig. 5a). The support particles have a shape of slightly flattened needles of size $l \times h = (50–150) \times (7–20)$ nm (on the average, approximately 70 × 10 nm), where l and h are the length and width of the needles, respectively (Fig. 5b). The EDX spectra suggest the presence of carbon in this sample with an average concentration of about 20 at % (to 50 at % in some sections of size ~100 nm as a result of their nonuniform distribution). The presence of carbon is due to the use of PVA in the synthesis of the support. For determining the reasons for the effect of heating on the sample synthesized in the presence of PVA, this sample was irradiated in situ with an electron beam in the microscope. Heating did not lead to a change in the overall sizes of the needle-shaped support particles and their aggregates; however, the structure became defective. This is reflected in the distortion of the needle shape of particles and the appearance of surface roughnesses (Figs. 5c, 5d).

Palladium in this sample predominantly occurred as isometric metal particles on the surface of large support pores (Fig. 5a). The active constituent was characterized by a polycrystalline structure: it consisted of aggregates formed by Pd nanoparticles with sizes of 2–5 nm. As a rule, the particles of Pd had a round shape; however, in certain cases, apparent signs of faceting manifested themselves (Fig. 5e). The HRTEM images (Fig. 5f) exhibit a lattice with a period of 0.225 nm, which corresponds to the metal interplanar spacing $d_{111} = 0.225$ nm. The particle size distribution of Pd (Fig. 5g) suggests the numerical predominance of particles with sizes of 20–30 nm; however, the distribution is sufficiently wide with the occurrence of multiblock particles with sizes to 200 nm. The average particle size of Pd in the Pd/Al_2O_3(PVA-110-N) sample was 30 nm. The bulk structure of Pd particles is weakly defective because of the presence of an insignificant amount of interblock boundaries in them (Fig. 5e). The pattern of electron diffraction by arbitrarily selected polycrystalline particles is ring-shaped due to

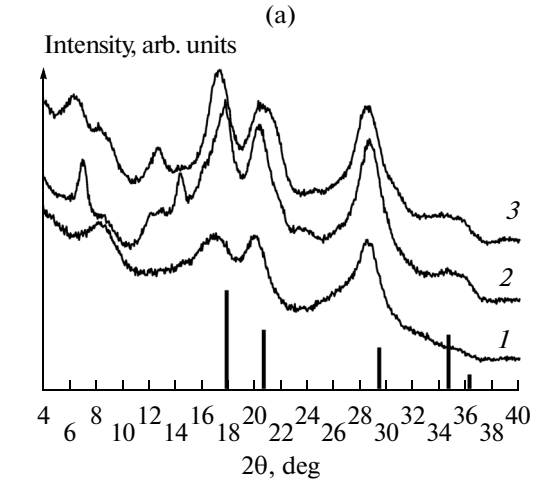

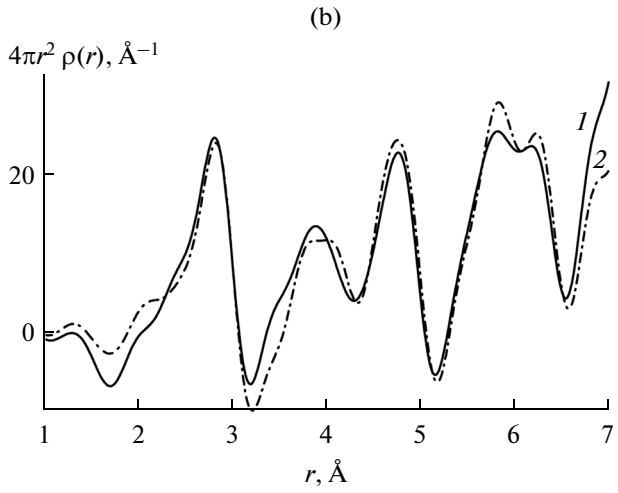

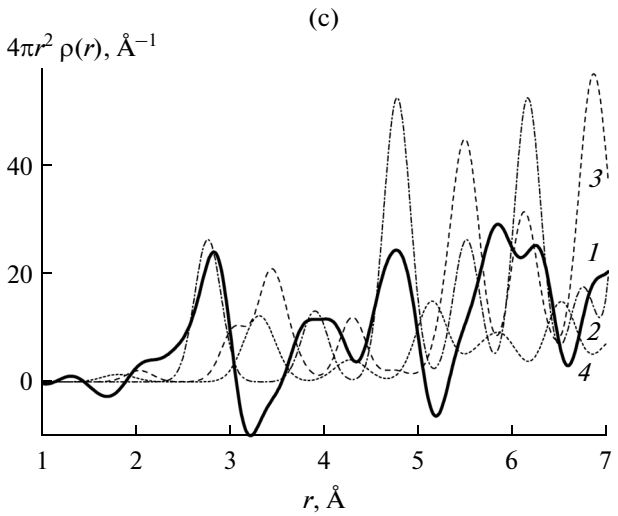

Fig. 4. X-ray diffraction analysis of the Al_2O_3(PVA-300-N) support and the Pd/Al_2O_3(PVA-300-N) catalyst: (a) diffraction patterns of (*1*) the support and the catalyst (*2*) before and (*3*) after CO oxidation obtained with the use of synchrotron radiation (vertical lines show the positions of the diffraction peaks of Pd^0, whose heights correspond to their relative intensities); (b) difference REDD curves of the catalyst (*1*) before and (*2*) after CO oxidation in the presence of water vapor; and (c) (*1*) the difference RAD curve of the catalyst after the reaction and the model RAD curves of (*2*) palladium metal, (*3*) the palladium oxide PdO, and (*4*) the environment of the Al^{3+} cation located in a tetrahedral position of the spinel structure of aluminum oxide.

the confluence of uniform reflections from individual polycrystals. The interplanar spacing of 0.225, 0.195, 0.114, 0.117 nm, etc., corresponds to Pd^0 (Fig. 5h).

According to the electron microscopic data, the Pd/Al_2O_3(PVA-300-N) sample consisted of supported Pd particles arranged on the surface and in the large pores of the Al_2O_3 support (Fig. 6a). The particles of Al_2O_3 have a shape of distorted needles with the same sizes as those in the Pd/Al_2O_3(PVA-110-N) sample, namely, (50–150) × (7–20) nm. From the TEM images, it follows that the Al_2O_3 particles in the Pd/Al_2O_3(PVA-300-N) sample have a defective structure. This is manifested in the loosening of particle surfaces, the appearance of mesopores in the bulk of the particles, and the partial structure amorphization (Fig. 6b). The oxidation of PVA under the conditions of sample calcination at 300°C can be the reason for the defect structure of support particles. The HRTEM image shows the disordered structure of Al_2O_3 near the edge of a particle (Fig. 6d). The EDX spectrum of the support particles indicates the presence of carbon on the needles in an amount consistent with the atomic ratio C : Al ≈ 10 : 90 (Fig. 6e). It is likely that amorphous carbon was localized in the above disordered layer on the surface of Al_2O_3 needles. Note that the specific surface area of Pd/Al_2O_3(PVA-300-N) is greater than the S_{BET} of the Pd/Al_2O_3(PVA-110-N) sample (Table 1); this is consistent with the observed changes in the morphology and structure of support particles.

In this sample, palladium was also present in the form of isometric metal particles arranged on Al_2O_3 (Fig. 6a). The HRTEM images of active constituent particles exhibit a metal lattice with the period d_{111} = 0.225 nm (Fig. 6f). The nanoparticles of palladium metal with a size of 1–3 nm also enter into the composition of Pd aggregates. The electron diffraction pattern also corresponds to Pd^0 (Fig. 6g). The survey TEM image (Fig. 6c), which was obtained at a low magnification (with the use of Z-contrast imaging in which the metal contrastingly appears against the background of the support), is indicative of the uniform size of palladium particles and the absence of anomalously large agglomerates. The size distribution of polycrystalline Pd particles is sufficiently narrow

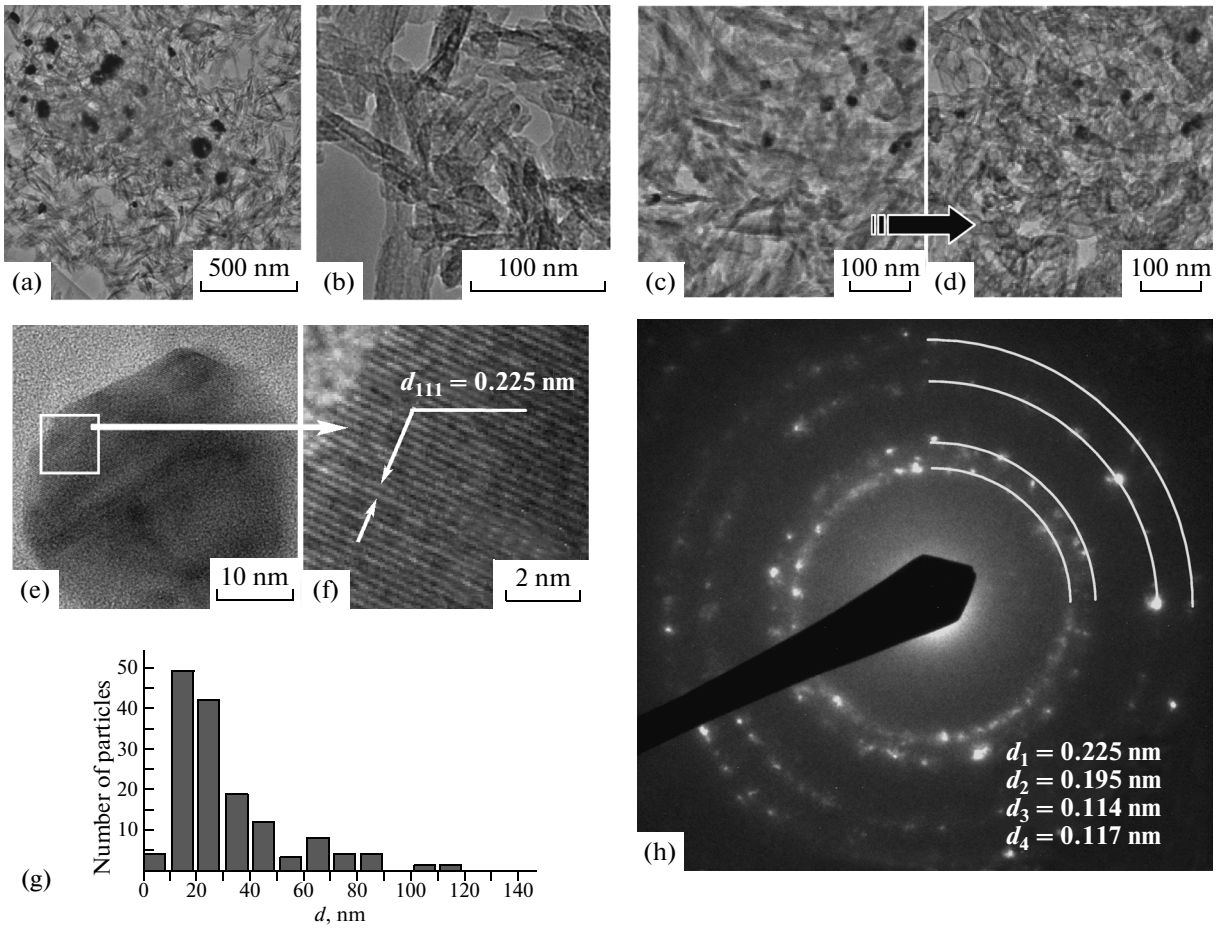

Fig. 5. Results of the electron microscopic study of the Pd/Al_2O_3(PVA-110-N) sample: (a) Pd particles on the surface of Al_2O_3; (b) the morphology of support particles; (c, d) TEM images of the same sample section (c) before and (d) after in situ electron-beam heating; (e) a Pd particle with a small number of interblock boundaries; (f) HRTEM image with the specified distance $d_{111} = 0.225$ nm of the metal; (g) Pd particle size distribution; and (h) electron diffraction by a polycrystalline Pd particle (interplanar spacing is indicated in descending order).

(Fig. 6h); quantitatively, particles with sizes of 20–30 nm predominate. The average Pd particle size in this sample is 25 nm. Thus, the supporting of palladium on Al_2O_3 treated at a higher temperature facilitates the formation of Pd^0; the average size of Pd aggregates is 25 nm.

The structure of the Pd/Al_2O_3(PVA-300-N) sample remained unchanged after performing CO oxidation on it, and it was almost identical to its structure before the reaction (Fig. 7a). The needle-shaped support particles had sizes of (50–150) × (7–20) nm; they were characterized by structural disorder analogous to that in the sample before the reaction. According to the EDX data, 10 at % carbon was present in Al_2O_3 (Fig. 7d). The particles of Pd^0 were located on the surface and in the large pores of support aggregates (Fig. 7a). The survey TEM image at a low magnification (Z-contrast imaging) (Fig. 7b) is indicative of the uniform size of palladium particles and the absence of anomalously large agglomerates. The results illustrated in Fig. 7c indicate the predominance of Pd particles with sizes of 20–30 nm; only very few particles had sizes below 70 nm. On the average, the particle size of Pd in this sample after reaction was 25 nm.

In terms of morphology, the active constituent particles were the aggregates of Pd nanoparticles with sizes of 5–10 nm (Fig. 7e). The HRTEM image (Fig. 7f) shows the lattice of several crystalline blocks, which are the constituents of a multiblock particle, with the period $d_{111} = 0.225$ nm, which corresponds to the metal.

The Pd/Al_2O_3(300-A) catalyst also consisted of supported Pd particles arranged on the support (Fig. 8). The support particles had a needle shape with sizes of (20–100) × (5–15) nm (Figs. 8a and 8b). In this sample (Fig. 8a), palladium particles on the support also formed aggregates with sizes of 25–150 nm, which consisted of Pd nanoparticles with sizes of 5–10 nm (Fig. 8c). Electron diffraction from the particles of palladium corresponds to its metallic state because a lattice with the period $d_{111} = 0.225$ nm is characteristic of the metal (Fig. 8c).

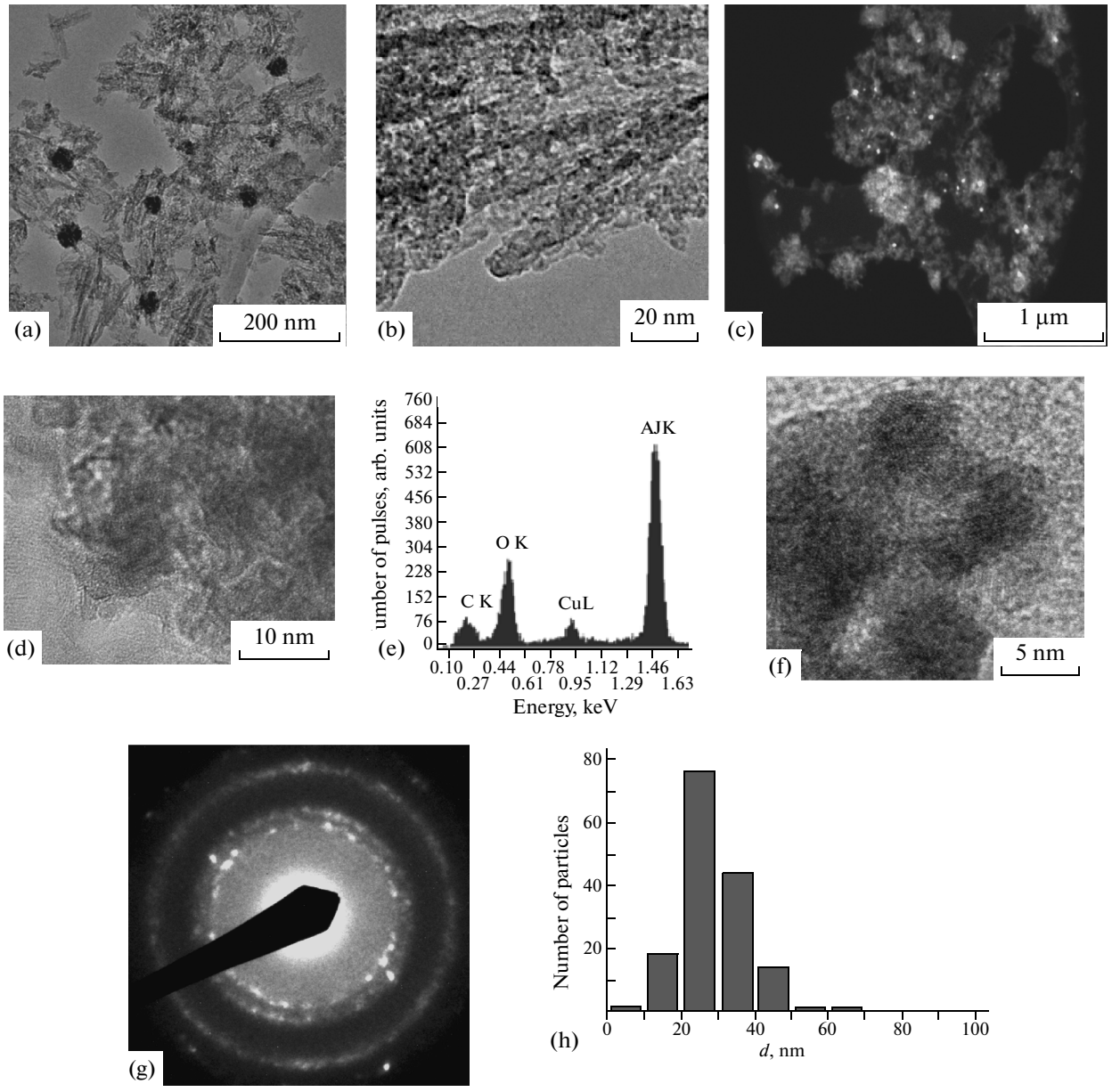

Fig. 6. Results of the electron microscopic study of the initial Pd/Al_2O_3(PVA-300-N) sample: (a) Pd particles on the surface of the Al_2O_3 support; (b) defective support particles; (c) low-resolution survey TEM image (Z-contrast imaging); (d) disordered Al_2O_3 structure near the particle edge; (e) EDX spectrum of support particles (the signal of carbon is present); (f) HRTEM image of a Pd particle; (g) electron diffraction from a polycrystalline Pd particle; and (h) Pd particle size distribution.

Thus, the electron-microscopic study of the Pd/Al_2O_3(PVA-110-N), Pd/Al_2O_3(PVA-300-N), and Pd/Al_2O_3(300-A) catalysts showed that the active constituent occurs as the aggregates of palladium metal nanoparticles on the surface of the supports, which have a shape of distorted needles and differ in carbon contents. In the Pd/Al_2O_3(PVA-300-N) sample, the sizes of aggregates and nanoparticles vary within ranges of 20–30 and 1–3 nm, respectively, whereas the aggregates and nanoparticles in the Pd/Al_2O_3(300-A) sample had sizes of 25–150 and 5–10 nm, respectively. In this case, the states and sizes of Pd particles remained almost unchanged after performing CO oxidation in the presence of water vapor.

Characterization of the Samples by Diffuse Reflectance Spectroscopy

The DRSs of the supports different in preparation conditions were reported elsewhere [21]. It was found that, on the surface of the supports obtained with the use of PVA, unsaturated oxygen-containing compounds (110°C), analogous compounds on the surface of polyene coke (300°C), or condensed aromatic coke

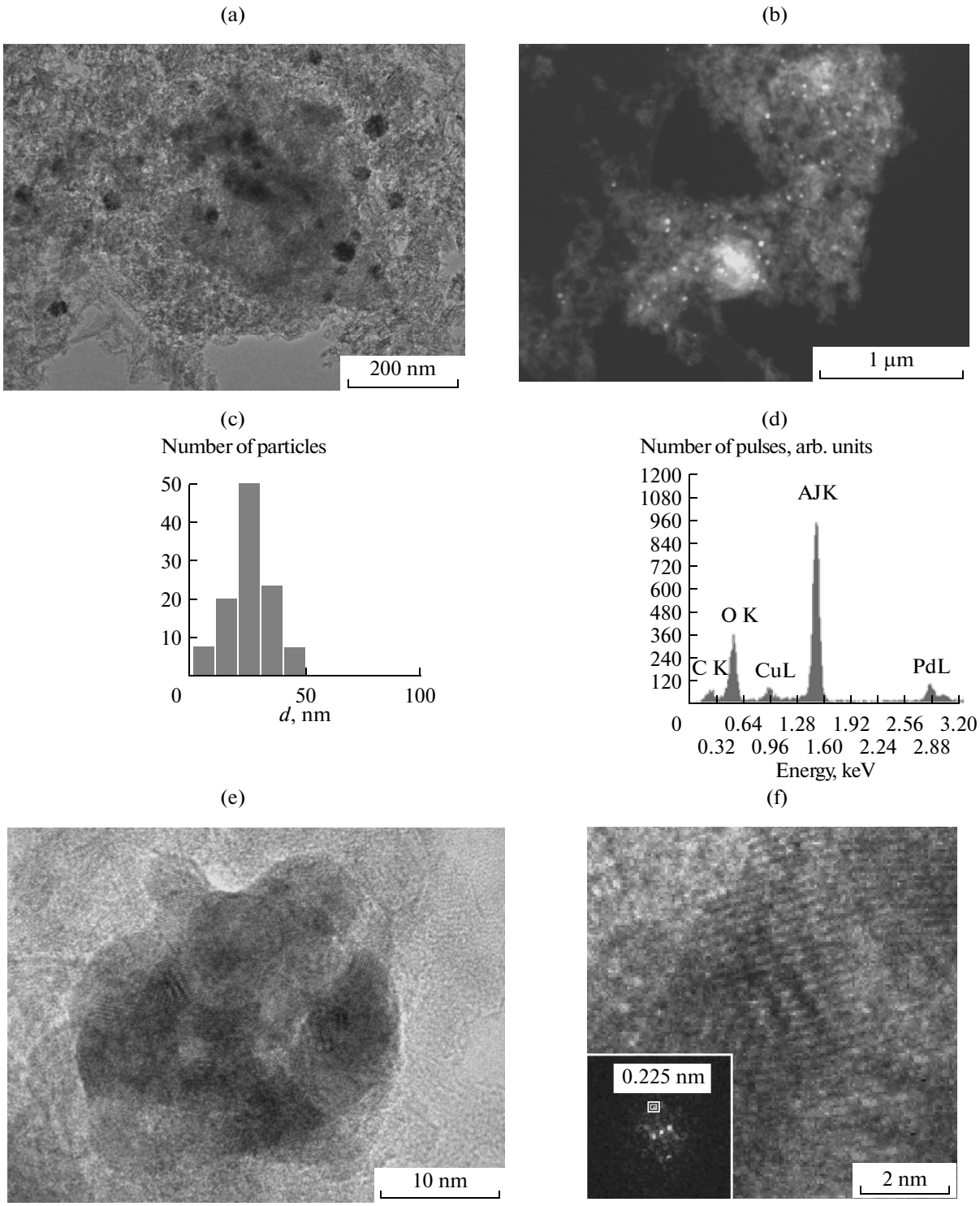

Fig. 7. Results of the electron microscopic study of the Pd/Al_2O_3(PVA-300-N) sample after the reaction: (a, b) the morphologies of Pd particles and the Al_2O_3 support (b, Z-contrast imaging); (c) Pd particle size distribution; (d) EDX spectrum of a sample section without a carbon layer background; (e) the block structure of a palladium particle; and (f) particle lattice planes with the spacing $d_{111} = 0.225$ nm, which corresponds to the metal.

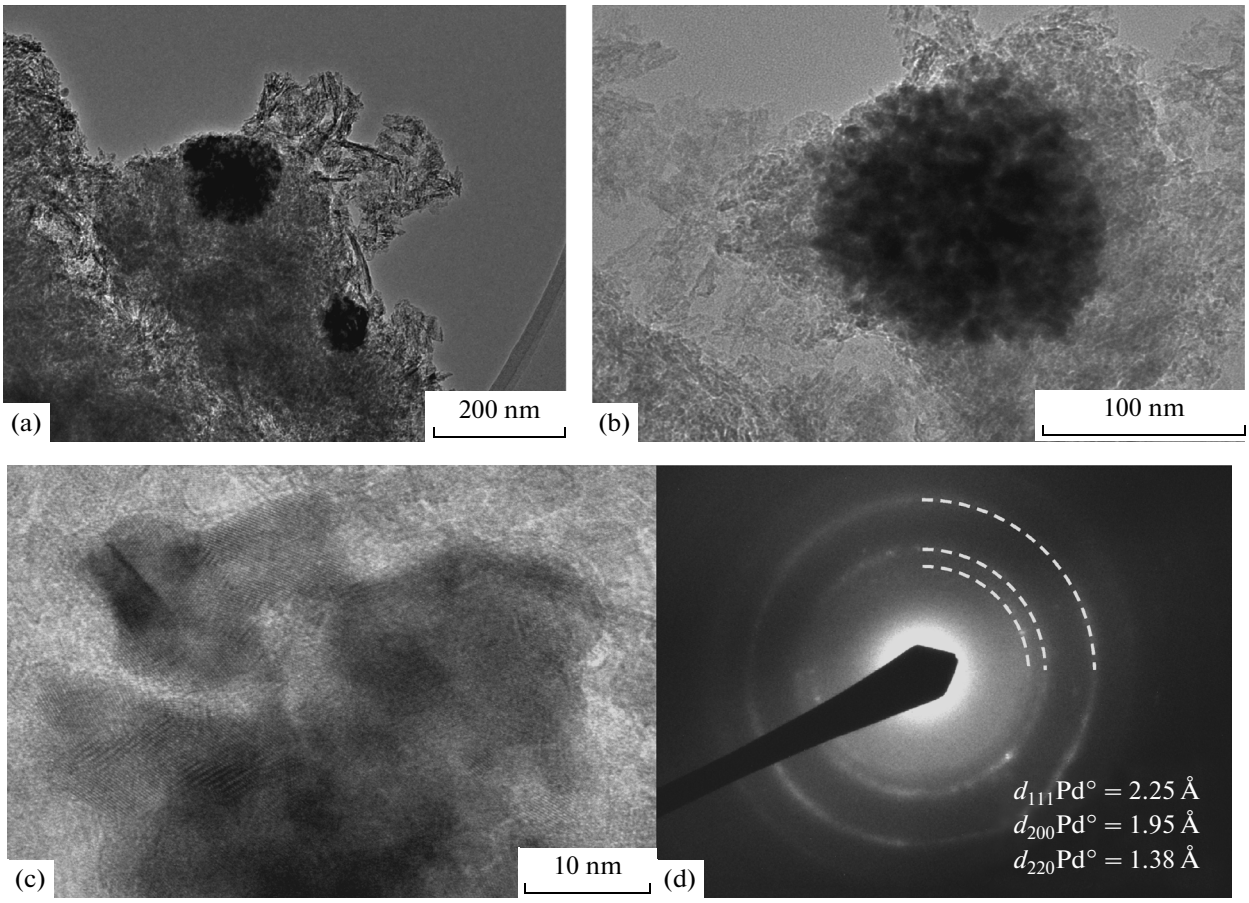

Fig. 8. Results of the electron microscopic study of the Pd/Al_2O_3(300-A) sample: (a, b) palladium particles of on the surface of the support; (c) HRTEM image of a Pd particle; and (d) electron diffraction from the aggregate of Pd particles.

(550°C) were present depending on the treatment temperature, whereas the surface of Al_2O_3(300-A) was free from carbon deposits.

Figure 9 shows the DRSs of the prepared catalysts with 1 wt % Pd. Unlike the spectra of the corresponding supports, the spectra of Pd/Al_2O_3(PVA-110-N) and Pd/Al_2O_3(PVA-300-N) do not contain intense absorption bands in a range of 46 000–50 000 cm^{-1}; this fact is indicative of the complete destruction of PVA with the formation of coke in the course of catalyst preparation. A weak band at 13 900 cm^{-1} due to the absorption of condensed coke on the support surface was almost absent from the spectra of the catalysts. The spectra of the Pd/Al_2O_3(PVA-T-N) catalysts did not contain absorption bands that could be attributed to Pd^{2+} both in isolated compounds and as a constituent of bulk palladium oxide [22, 23].

Unlike the above spectra, an intense absorption band at 47 000–50 000 cm^{-1} appeared in the spectrum of the Pd/Al_2O_3(300-A) sample (Fig. 9, curve *4*a); this band can be attributed to the resonance absorption of electromagnetic radiation by Pd^0 particles (plasmon absorption). According to the calculations carried out in accordance with the Mie theory [24], the optical spectrum of small colloidal particles of Pd^0 exhibits a wide absorption band at 50 000 cm^{-1}, whose intensity smoothly decreases toward the long-wave region. An absorption band in the above region was also observed in the spectrum of Pd foil (Fig. 9, curve *5*a).

The spectra of the Pd/Al_2O_3 (PVA-T-N) samples exhibited structureless absorption characterized by a strong increase in intensity in the long-wavelength region (Fig. 9, curves *1*a–*3*a). This is indicative of the presence highly dispersed palladium metal or palladium black on the surface [3, 22]. Obviously, the high intensity of absorption in the long-wavelength region of the spectrum is related to light scattering by metal particles. It is well known that the intensity of light scattering by small particles whose size is smaller than the wavelength of light is proportional to their size. An analysis of data shown in Fig. 9 allowed us to assume that palladium metal particles in the Pd/Al_2O_3(PVA-300-N) sample, whose support is covered with polyene coke, exhibited a minimal size. The action of the reaction mixture on the Pd/Al_2O_3(PVA-110-N), Pd/Al_2O_3(PVA-300-N), and Pd/Al_2O_3(PVA-550- N) catalysts at 20°C in the presence of water did not cause changes in the shape of DRSs (Fig. 9) or the appear-

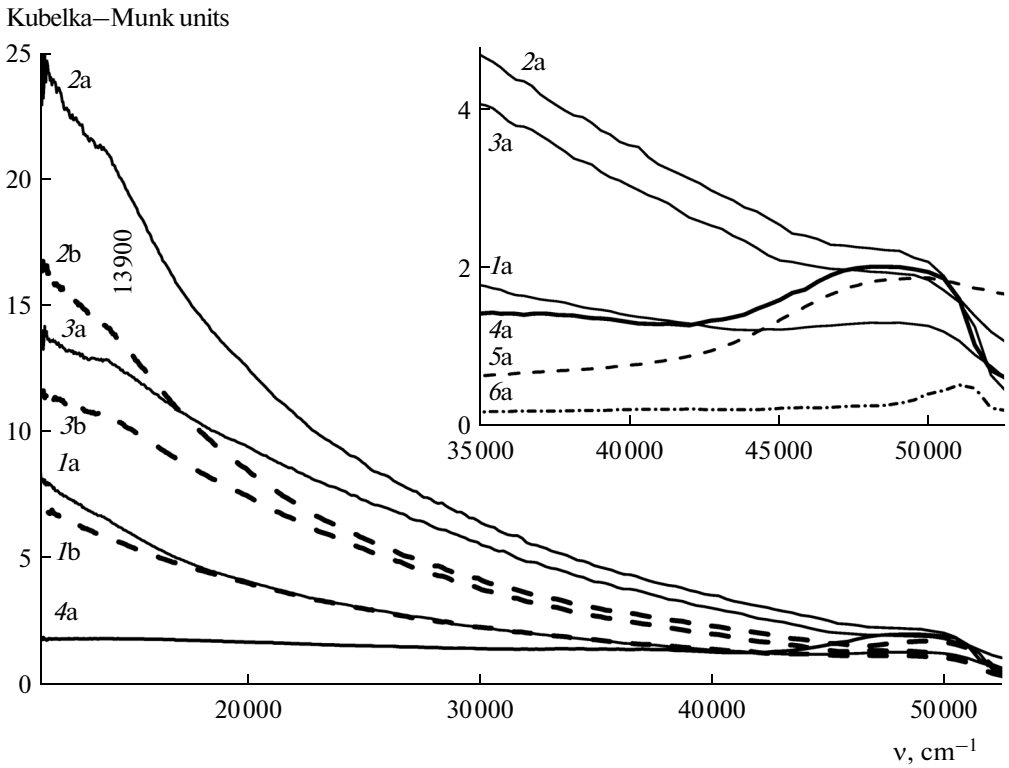

Fig. 9. DRSs of the samples of (*1*) Pd/Al_2O_3 (PVA-110-N), (*2*) Pd/Al_2O_3(PVA-300-N), (*3*) Pd/Al_2O_3(PVA-550-N), (*4*) Pd/Al_2O_3(300-A), (*5*) Pd foil, and (*6*) Al_2O_3(300-A) (a) before and (b) after the reaction.

ance of new absorption bands. Consequently, the state of palladium in these catalytic systems remained unchanged after conducting CO oxidation.

Characterization of the Samples by XPS

The study of the freshly prepared supported catalysts by XPS showed (Table 3) that they contained only a carbon impurity in a sufficiently large amount. In this case, the ratio between the surface atomic concentrations of carbon and aluminum decreased from 3.51 to 0.71 as the support treatment temperature was increased; that is, the surface of the Pd/Al_2O_3(PVA-110-N) sample was enriched in carbon to the greatest degree. The C/Al ratios in the Pd/Al_2O_3(PVA-300-N) and Pd/Al_2O_3(300-A) samples were close to each other.

Note that the concentration of palladium on the catalyst surfaces was very low with respect to aluminum oxide (0.01–0.04%) at a specified concentration of 1 wt %; this can be explained by the presence of a large amount of carbon capable of screening palladium.

According to the XRD data, the presence of sodium in the test catalysts is related to the occurrence of sodium aluminum hydroxycarbonate $NaAlCO_3(OH)_2$, which was formed at the stage of the preparation of catalysts on the treatment of them with sodium formate. Table 3 indicates that the greatest amount of sodium (~2 at %) occurred on the surface of Pd/Al_2O_3(PVA-110-N). This amount in the Pd/Al_2O_3(PVA-300-N) sample was smaller by a factor of about 4, and it increased again in Pd/Al_2O_3(PVA-550-N). It is likely that the surface concentration of sodium changed due to different specific surface areas of the catalysts because the surface concentrations of Na in the Pd/Al_2O_3(PVA-110-N) and Pd/Al_2O_3(PVA-550-N) samples were almost the same: 0.04×10^{20} and 0.05×10^{20} atom/m^2, respectively.

The presence of nitrogen on the surface was caused by the use of DMF at the stage of catalyst preparation, although the Pd/Al_2O_3(PVA-550-N) sample did not contain nitrogen. From the experimental results, it follows that DMF did not remain on the surface of aluminum oxide calcined at 550°C when it is considered that the catalysts were only dried at room temperature.

The elemental surface composition and the concentrations of the main components in the Pd/Al_2O_3(PVA-300-N) catalyst after the action of the reaction medium containing water vapor changed insignificantly (Table 3); this fact is indicative of the stability of the catalyst under reaction conditions.

Figure 10 shows the Pd3*d* XPS spectra of the Pd/Al_2O_3(PVA-T-N) and Pd/Al_2O_3(300-A) catalysts, which characterize the charge state of palladium. The line of palladium in the spectra of Pd/Al_2O_3(PVA-T-N)

Table 3. Elemental composition of the surfaces of the supported catalysts

Sample	Concentration, at %						C/Al
	C	O	Pd	Al	N	Na	
Pd/Al_2O_3(PVA-110-N)	27.4	57.5	0.01	7.8	5.30	2.01	3.51
Pd/Al_2O_3(PVA-300-N)	17.7	66.7	0.03	14.4	0.71	0.47	1.23
Pd/Al_2O_3(PVA-300-N)*	18.4	66.5	0.04	13.9	0.61	0.60	1.32
Pd/Al_2O_3(PVA-550-N)	11.8	70.5	0.02	16.6	0	1.11	0.71
Pd/Al_2O_3(300-A)	23.9	59.1	–	16.1	0.88	–	1.48

* After the reaction in the presence of H_2O.

(Fig. 10, curves *1–3*) is described by one spin–orbital doublet with a Pd3$d_{5/2}$ binding energy of 335.8 eV. Although the line is widened, it would be incorrect to recognize two or more states of palladium (if any) because of a weak signal intensity and unresolved line. A peak maximum with E_b = 335.8 eV formally corresponds to small palladium clusters of size ~1 nm or smaller [25, 26]. We failed to detect the Pd3*d* line in the spectrum of the Pd/Al_2O_3(300-A) reference sample (Fig. 10, curve *4*); this fact suggests the absence of palladium detectable by XPS analysis.

An analysis of the spectrum (which is not presented here) of the Pd/Al_2O_3(PVA-300-N) supported catalyst after conducting CO oxidation on it in the presence of water vapor showed that a peak at 335.8 eV corresponds to Pd^0 nanoparticles, as in the initial state. Thus, palladium in the supported catalysts did not undergo substantial changes under the action of the reaction atmosphere.

Based on the experimental results, we can conclude that the total Pd3*d* line intensity in the spectra of the Pd/Al_2O_3(PVA-T-N) samples is sufficiently low, and it corresponds to a palladium concentration of 0.01–0.04 at %, which is lower than the specified value by almost two orders of magnitude. The Pd3*d* line is absent from the spectrum of Pd/Al_2O_3(300-A). The low intensity of the Pd3*d* line or its absence can be caused by the formation of large palladium aggregates (or particles) and/or by the decoration of palladium particles with the support.

As noted above, the position of the Pd3*d* line in the spectra of the Pd/Al_2O_3(PVA-T-N) samples formally corresponds to small metal clusters of size ~1 nm or smaller. However, the results of studying the samples by structural analysis methods (XRD analysis and HRTEM) indicated the presence of large palladium aggregates with sizes of hundreds of nanometers, which consisted of Pd^0 nanoparticles of sizes 2–10 nm. The Pd3$d_{5/2}$ binding energy in these metal particles should be close to E_b in the compact metal (335.2 eV). The higher Pd3*d* binding energy of 335.8 eV can be explained by physical effects in the measurement of the XPS spectra. If palladium aggregates are decorated with the support, this leads to the blocking of their contact with the background inelastic electron scattering in the analytical chamber of the spectrometer. As a consequence, the potential produced on the test particles under the action of X-radiation differs from the surface potential of the support and carbon on its surface, whose C1*s* line was used for the calibration of XPS spectra. Therefore, the observed Pd3*d* binding energy, which is increased in comparison with E_b in compact palladium metal, can be explained by the impossibility of accurately calibrating the Pd3*d* spectra based on the C1*s* line of surface carbon.

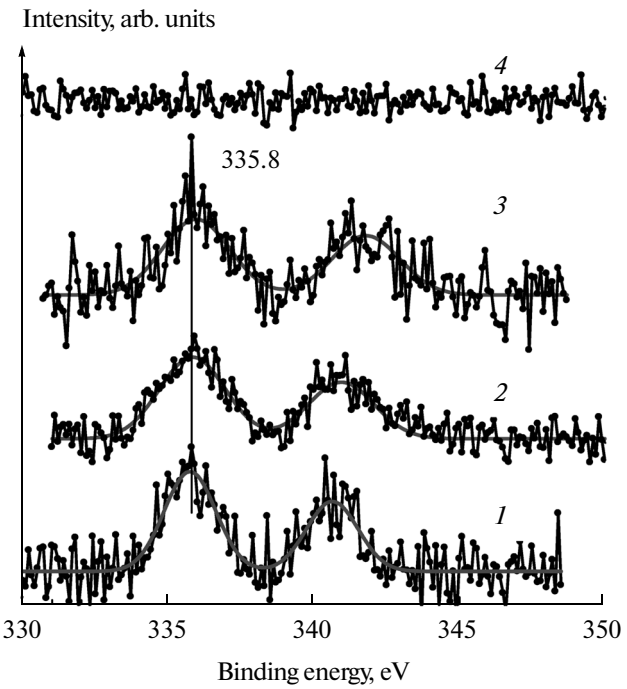

Fig. 10. The Pd3*d* photoelectron spectra of the (*1*) Pd/Al_2O_3(PVA-110-N), (*2*) Pd/Al_2O_3(PVA-300-N), (*3*) Pd/Al_2O_3(PVA-550-N), and (*4*) Pd/Al_2O_3(330-A) samples.

CONCLUSIONS

Thus, the study of the supported Pd-containing catalysts different in the preparation conditions and treatment temperatures of a support based on aluminum oxide showed that they were similar in terms of activity under the TPR conditions of CO oxidation: the T_{50} temperatures for the Pd/Al_2O_3(PVA-300-N) and Pd/Al_2O_3(300-A) samples were 142 and 165°C, respectively. More significant differences were observed when CO oxidation was performed under isothermal conditions at room temperature in the absence and in the presence of water vapor in the reaction mixture. Pd/Al_2O_3(PVA-300-N) exhibited the highest activity: in the absence of water, the initial conversion of CO was 40%; then, it gradually decreased. In the presence of water vapor, the conversion of CO continuously increased to 88% and stabilized at this level. In all of the catalysts, palladium occurred in a metallic state, which was also retained after catalyst testing in the reaction of CO oxidation at room temperature in the presence of water vapor. The observed differences can be explained by the following reasons:

First, this is the unequal dispersity of palladium metal, which decreases in the order Pd/Al_2O_3(PVA-300-N) > Pd/Al_2O_3(PVA-110-N) > Pd/Al_2O_3(300-A). This is confirmed by the results of studying the samples by structural analysis methods. According to the XRD analysis data, the size of palladium metal crystallites in the Pd/Al_2O_3(PVA-300-N) and Pd/Al_2O_3(300-A) catalysts does not exceed 1 and 5 nm, respectively. However, according to the HRTEM data, palladium in these catalysts predominantly occurs as the aggregates of Pd nanoparticles; the sizes of the aggregates and the nanoparticles in the Pd/Al_2O_3(PVA-300-N), Pd/Al_2O_3(PVA-110-N), and Pd/Al_2O_3(300-A) samples are 25 and 1–3, 30 and 2–5, and 25–150 and 5–10 nm, respectively. Furthermore, according to the results obtained by diffuse reflectance spectroscopy, the most highly dispersed palladium was present in the Pd/Al_2O_3(PVA-300-N) sample.

Second, this is the different state of support surfaces: unsaturated oxygen-containing compounds (110°C), polyene coke (300°C), or condensed coke (550°C) were present on the surface of Al_2O_3(PVA-T-N) depending on treatment temperature, whereas the surface of Al_2O_3(300-A) was free from carbon deposits. According to the XPS data, the C/Al ratio in the Al_2O_3(PVA-T-N) samples decreased in the order Pd/Al_2O_3(PVA-110-N) (3.5) > Pd/Al_2O_3(PVA-300-N) (1.3) > Pd/Al_2O_3(PVA-550-N) (0.7). If we take into account that the surface area occupied by a C atom is 0.04×10^{-18} m^2 [27], the carbon monolayer coverage is 0.25×10^{20} atom/m^2. In the Pd/Al_2O_3(PVA-110-N) and Pd/Al_2O_3(PVA-300-N) samples, the surface concentration of carbon was $\sim 0.20 \times 10^{20}$ atom/m^2, which is close to the monolayer coating. However, carbon in Pd/Al_2O_3(PVA-110-N) occurred as a constituent of unsaturated oxygen-containing compounds, which may block active sites to make them less accessible to reaction mixture components. It is likely that the presence of polyene coke on the surface of Pd/Al_2O_3(PVA-300-N) in an amount close to the monolayer coating creates less steric hindrances for the access of these components to palladium metal. Note that, according to Shen et al. [4], the oxidation of CO on the Pd–Cu–Cl_x/Al_2O_3 catalyst at room temperature in the presence of water vapor was accompanied by a decrease in the conversion of CO because of the capillary condensation of water on the hydrophilic Al_2O_3 support. Therefore, the presence of surface carbon in the form of polyene coke ensures the hydrophobicity of the support to increase the stability of the Pd/Al_2O_3(PVA-300-N) catalyst under reaction conditions.

Third, according to the RAD data, OH groups were formed on the surface of the Pd/Al_2O_3(PVA-300-N) catalyst in the presence of water vapor as a result of the hydration of the support. It is likely that they differ in chemical properties from the OH groups formed on the initial support in the course of catalyst preparation. The results of CO oxidation on the Pd/Al_2O_3(300-A) catalyst at room temperature in the presence of water vapor count in favor of this hypothesis: the conversion of CO at the initial point in time was ~50%; thereafter, it rapidly decreased rather than increased as on the Pd/Al_2O_3 (PVA-300-N) catalyst. The role of hydroxyl groups in the low-temperature process of CO oxidation was reported in a number of publications [28–31]. According to Kunkalekar and Salker [32] and Shido and Iwasawa [33], in the presence of OH groups, an additional reaction path of the interaction of CO with OH groups can occur: water that is present in the reaction mixture is dissociatively adsorbed to produce OH^- and H^+ species. The OH^- species interact with CO to form intermediates like surface bicarbonates or formates, which are then decomposed into CO_2 and hydrogen. On the other hand, according to Zhai et al. [34], the presence of alkali metals increases the concentration of OH groups and facilitates their localization, for example, near palladium atoms to affect the strength of their bond and reactivity. Therefore, their subsequent interaction with CO adsorbed on the particles of palladium occurs with a high rate and a low activation energy. However, an analysis of data summarized in Table 3 showed that a direct relationship between the activity and the surface concentration of sodium was not observed: the Pd/Al_2O_3(PVA-300-N) catalyst containing ~0.5 at % Na was more active than Pd/Al_2O_3(PVA-550-N) which contained ~1.1 at % Na.

Thus, the activity of the Pd/Al_2O_3 catalyst in CO oxidation at room temperature in the presence of water vapor depends on the size of palladium metal nanoparticles, the presence of a nearly monolayer coating with surface carbon, and the presence of OH groups formed because of the dissociation of water, which is present in the reaction mixture.

REFERENCES

1. Ivanova, A.S., Slavinskaya, E.M., Stonkus, O.A., Zaikovskii, V.I., Danilova, I.G., Gulyaev, R.V., Bulavchenko, O.A., Tsybulya, S.V., and Boronin, A.I., *Kinet. Catal.*, 2013, vol. 54, no. 1, p. 81.
2. Martínez-Arias, A., Hungría, A.B., Fernández-García, M., Iglesias-Juez, A., Anderson, J.A., and Conesa, J.C., *J. Catal.*, 2004, vol. 221, p. 85.
3. Ivanova, A.S., Slavinskaya, E.M., Gulyaev, R.V., Zaikovskii, V.I., Danilova, I.G., Plyasova, L.M., Polukhina, I.A., and Boronin, A.I., *Appl. Catal., B*, 2010, vol. 97, nos. 1–2, p. 57.
4. Shen, Y., Lu, G., Guo, Y., and Wang, Y., *Chem. Commun.*, 2010, vol. 46, p. 8433.
5. Utamapanya, S., Klabunde, K.J., and Schlup, J.P., *Chem. Mater.*, 1991, vol. 3, no. 1, p. 175.
6. Diao, Y., Walawender, W.P., Sorensen, Ch.M., Klabunde, K.J., and Ricker, T., *Chem. Mater.*, 2002, vol. 14, no. 1, p. 362.
7. Thoms, H., Epple, M., and Reller, A., *Solid State Ionics*, 1997, vols. 101–103, p. 79.
8. Zou, Z.-Q., Meng, M., Guo, L.-H., and Zha, Y.-Q., *J. Hazard. Mater.*, 2009, vol. 163, p. 835.
9. Price, W.J., *Analytical Atomic Absorption Spectroscopy*, London: Heyden, 1972.
10. *PCPDFWin, Ver. 1.30*, Swarthmore, Penn.: JCPDS ICDD, 1997.
11. Moroz, E.M., *Russ. Chem. Rev.*, 2011, vol. 80, no. 4, p. 293.
12. Moroz, E.M., Zyuzin, D.A., and Shefer, K.I., *J. Struct. Chem.*, 2007, vol. 48, no. 2, p. 262.
13. Buyanova, N.E., Karnaukhov, A.P., and Alabuzhev, Yu.A., *Opredelenie udel'noi poverkhnosti dispersnykh i poristykh materialov* (Determination of the Specific Surface Area of Dispersed and Porois Materials), Novosibirsk: Inst. Kataliza, 1978.
14. Boehm, H.-P. and Knozinger, H., in *Catalysis Science and Technology*, Anderson, J.R. and Boudart, M, Eds., Berlin: Springer, 1983, vol. 4, p. 39.
15. Slavinskaya, E.M., Chesalov, Yu.A., Boronin, A.I., Polukhina, I.A., and Noskov, A.S., *Kinet. Catal.*, 2005, vol. 46, p. 555.
16. Titkov, A.I., Salanov, A.N., Koscheev, S.V., and Boronin, A.I., *React. Kinet. Catal. Lett.*, 2005, vol. 86, p. 371.
17. Knyazev, A.S., Magaev, O.V., Vodyankina, O.V., Titkov, A.I., Salanov, A.N., Koshcheev, S.V., and Boronin, A.I., *Kinet. Catal.*, 2005, vol. 46, p. 151.
18. *Handbook of X-Ray Photoelectron Spectroscopy*, Moulder, J.F., Stickle, W.F., and Sobol, P.E., Eds., Eden Prairie, Minn.: PerkinElmer, 1992.
19. Ivanova, A.S., Litvak, G.S., Kryukova, G.N., Tsybulya, S.V., and Paukshtis, E.A., *Kinet. Catal.*, 2000, vol. 41, no. 1, p. 122.
20. Ushakov, V.A., Moroz, E.M., and Levitskii, E.A., *Kinet. Katal.*, 1985, vol. 26, p. 1200.
21. Korneeva, E.V., Ivanova, A.S., Zyuzin, D.A., Moroz, E.M., Stonkus, O.A., Zaikovskii, V.I., and Danilova, I.G., *Kinet. Catal.*, 2012, vol. 53, no. 4, p. 440.
22. Rakai, A., Tessier, D., and Bozon-Verduraz, F., *New J. Chem.*, 1992, vol. 16, p. 869.
23. Lyubovski, M. and Pfefferle, L., *Catal. Today*, 1999, vol. 47, nos. 1–4, p. 29.
24. Creighton, J.A. and Eadon, D.G., *J. Chem. Soc., Faraday Trans.*, 1991, vol. 87, p. 3881.
25. Wertheim, G.K., *Z. Phys. D: At. Mol. Clusters*, 1989, vol. 12, nos. 1–4, p. 319.
26. Mason, M.G., *Phys. Rev. B*, 1983, vol. 27, no. 2, p. 748.
27. Satterfield, Ch., *Heterogeneous Catalysis in Practice*, New York: McGraw-Hill, 1980.
28. Cunningham, D.A.H., Kobayashi, T., Kamijo, N., and Haruta, M., *Catal. Lett.*, 1994, vol. 25, p. 257.
29. Calla, J.T. and Davis, R., *J. Ind. Eng. Chem. Res.*, 2005, vol. 44, p. 5403.
30. Costello, C.K., Yang, J.H., Law, H.Y., Wang, Y., Lin, J.N., Marks, L.D., Kung, M.C., and Kung, H.H., *Appl. Catal., A*, 2003, vol. 243, p. 15.
31. Haruta, M.J., *New Mater. Electrochem. Syst.*, 2004, vol. 7, p. 163.
32. Kunkalekar, R.K. and Salker, A.V., *Catal. Commun.*, 2010, vol. 12, p. 193.
33. Shido, T. and Iwasawa, Y., *J. Catal.*, 1993, vol. 141, no. 1, p. 71.
34. Zhai, Y.P., Pierre, D., Si, R., Deng, W.L., Ferrin, P., Nilekar, A.U., Peng, G.W., Herron, J.A., Bell, D.C., Saltsburg, H., Mavrikakis, M., and Flytzani-Stephanopoulos, M., *Science*, 2010, vol. 329, p. 1633.

Translated by V. Makhlyarchuk